ARMY RESEARCH LABORATORY

The Spatial Coherence of Electron Wavefunctions and the Transition from Miniband to Stark-Ladder Electric Field Regimes in InGaAs/InAlAs-on-InP Superlattices

by John L. Bradshaw and Richard P. Leavitt

ARL-TR-1536

February 1998

The findings in this report are not to be construed as an official Department of the Army position unless so designated by other authorized documents.

Citation of manufacturer's or trade names does not constitute an official endorsement or approval of the use thereof.

Destroy this report when it is no longer needed. Do not return it to the originator.

Army Research Laboratory
Adelphi, MD 20783-1197

ARL-TR-1536 **February 1998**

The Spatial Coherence of Electron Wavefunctions and the Transition from Miniband to Stark-Ladder Electric Field Regimes in InGaAs/InAlAs-on-InP Superlattices

John L. Bradshaw and Richard P. Leavitt
Sensors and Electron Devices Directorate

Abstract

Five $In_{0.53}Ga_{0.47}As/In_{0.52}Al_{0.48}As$-on-InP superlattices of various well-to-barrier ratios and miniband widths have been studied by low-temperature photoluminescence, photocurrent, and differential photocurrent spectroscopies. These techniques provide a means of measuring the spatial coherence length of electron wavefunctions in the superlattices. We find that the onset of Wannier-Stark localization occurs when the well-to-well potential drop within the superlattice is between 1.1 and 1.43 times the low-temperature photoluminescence linewidth for all samples studied. Furthermore, the photoluminescence linewidth is accurately describable in terms of a simple model for alloy broadening. These findings confirm an intuitive picture for the transition between the miniband and Wannier-Stark electric field regimes in $In_{0.53}Ga_{0.47}As/In_{0.52}Al_{0.48}As$-on-InP superlattices.

Contents

Figures

Table

1. Introduction

The optical and electronic properties of superlattices are of interest to the Army because of the profound effects of superlattices on the operational performance of numerous state-of-the-art optoelectronic and photonic devices. For example, bound-to-miniband quantum-well infrared photodetectors (QWIPs) [1], infrared hot-electron transistors [2], and Wannier-Stark modulators [3] are all devices that both explicitly exploit various advantageous properties of superlattices and are being actively pursued as components in next-generation Army optoelectronic and photonic systems.

This technical report focuses on two aspects of superlattices relevant to their effect on device performance: the superlattice spatial coherence length and the transition from the miniband to the Wannier-Stark ladder electric field regimes. The spatial coherence length is simply the physical extent of the electron wavefunction along the growth direction of the superlattice. Figure 1(a) shows a simplified diagram of a superlattice miniband. When the applied electric field is zero and the barriers between quantum wells are sufficiently thin, the electrons are in principle delocalized throughout the entire superlattice, and the band structure (at $k_{\|} = 0$) takes the form of the superlattice miniband shown. At small values of applied electric field, the electrons become localized, but the wavefunction can extend over many superlattice periods. A simple semiclassical picture predicts that the electron becomes localized within a region Δ/eF, where Δ is the superlattice miniband width, e is the magnitude of the electron charge, and F is the electric field. This is the Wannier-Stark regime, shown schematically in figure 1(b). At high electric fields, the wavefunctions become completely localized into one quantum well. This regime is shown schematically as figure 1(c).

Recently, we used photoluminescence (PL), photocurrent (PC), and differential photocurrent spectroscopies at low temperature to study the spatial coherence of electrons in a 30-Å $In_{0.53}Ga_{0.47}As$/20-Å $In_{0.52}Al_{0.48}As$ superlattice [4] grown lattice-matched to InP. We learned two important things from this study. First, we measured the PL linewidth at 2 K to be 4.3 meV and found that this linewidth was consistent with the minimum linewidth calculated for an exciton in a semiconductor-alloy superlattice, assuming that the alloy cations are randomly distributed on the group III lattice sites. Second, the longest spatial coherence length measured was 1450 Å at 2 K. This coherence length corresponds to a well-to-well potential drop of 4.9 meV, almost exactly the alloy-broadened linewith measured in PL.

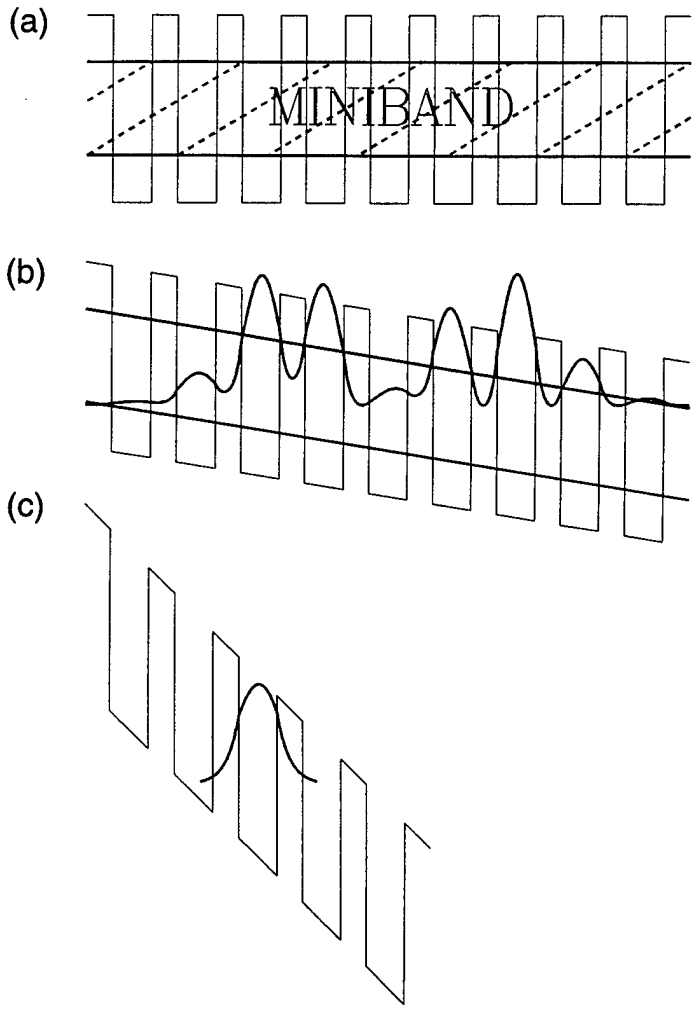

Figure 1. Three electric field regimes of a semiconductor superlattice: (a) miniband regime, (b) Wannier-Stark regime, and (c) high-field regime. In (b) and (c), the electron envelope wavefunctions (squared) are shown; the wavefunction in (b) extends over many superlattice periods and diminishes toward zero, in rough agreement with the classically predicted turning points at the edges of the miniband.

The results of this study suggested a simple intuitive model for the spatial coherence of the electron and the transition from the miniband to the Wannier-Stark ladder electric field regimes. This model is explained briefly as follows. In a real superlattice, the random fluctuations of the alloy potential and the layer thickness fluctuations that underlie the measured PL linewidth create a random potential contribution to the periodic potential of the superlattice. This random potential localizes electronic states that at zero electric field would extend throughout the superlattice. Thus for a real superlattice, the electric field effects associated with the Wannier-Stark electric field regime would be observed only when the Stark-localization length Δ/eF is smaller than the coherence length of the electronic states localized by the random potential. The electric field causing the transition between miniband and Wannier-Stark electric field regimes is then defined operationally as the smallest electric field for which the Stark-localization length is smaller than the coherence length of the electronic states localized by the random potential.

The physical model for Stark localization explained above, although intuitively appealing, is based on measurements of only one sample. The results presented below test this model for a wider range of well-to-barrier ratios and several miniband widths. We find that every sample studied shows a transition from the miniband regime to the Wannier-Stark regime in correspondence with the model described above.

2. Sample Description and Experimental Technique

Figure 2 is a contour plot of miniband width versus superlattice barrier-to-period ratio for $In_{0.53}Ga_{0.47}As/In_{0.52}Al_{0.48}As$ superlattices. Each contour is drawn for a given period P. Figure 2 was generated with a simple Kronig-Penney model (including band-nonparabolicity effects [5]) for the miniband width. The strategy adopted was to study a series of samples of various miniband widths (samples a, e, and c in fig. 2) and also to study two pairs of samples (pairs a-b and c-d in fig. 2) in which both samples of a given pair had nearly identical miniband widths but widely disparate barrier-to-period ratios.

The samples were grown by molecular-beam epitaxy (MBE) on n-doped InP substrates and consisted of 0.25 μm of n-doped (In,Al)As buffer layer followed by 0.1 μm of undoped (In,Al)As, 0.8 μm of undoped superlattice, another 0.1 μm of undoped (In,Al)As, 0.2 μm of p-doped (In,Al)As, and a 200-Å p-doped (In,Ga)As capping layer. All layers were grown nominally lattice matched to the InP. High-resolution x-ray diffraction spectra ((004) reflection) on sample c showed a high degree of structural perfection. Near

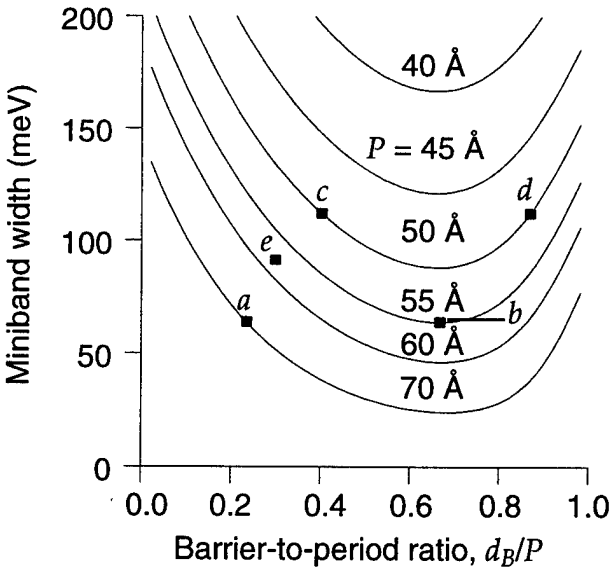

Figure 2. Contour plot of miniband width Δ versus superlattice barrier-to-period ratio d_B/P for $In_{0.53}Ga_{0.47}As/In_{0.52}Al_{0.48}As$-on-InP superlattices. Each contour is drawn for a given period P. Black squares indicate samples considered in this study.

the (004) InP substrate reflection, the x-ray peaks of the substrate, thick (In,Al)As layers, and superlattice overlap and cannot be individually resolved; we conclude that the average mismatches of these layers must be less than 2×10^{-4}. The first-order satellites in the x-ray spectrum have a full width at half maximum (FWHM) of 23 arc seconds, which is exactly the width that we calculated for these peaks for our diffractometer using dynamical diffraction theory and assuming a perfect structure. From the x-ray data, we conclude that the rms well-width fluctuations for sample *e* are less than 0.02 monolayers (0.06 Å). The other samples were grown under MBE growth conditions that were nearly identical to those for sample *c*, and we therefore expect similar structural quality for these samples.

The PL measurements were conducted with the sample immersed in liquid He pumped below the λ point. The He bath temperature was nominally 2 K. The samples were excited with Ar^+ laser radiation at 514.5 nm and an excitation intensity in the range of 0.1 to 1.0 W/cm^2. The PL signal was optically chopped, dispersed through a 2/3-m monochromator and detected with an InAs photovoltaic detector. The detected signal was processed by conventional lock-in techniques. For PC measurements, the samples were processed into 500-μm-diameter mesa diodes with ring contacts. Chopped light dispersed through a 3/4-m monochromator was focused onto one of the diodes, and the resulting PC signal was measured with a lock-in amplifier. For differential PC measurements, the monochromator wavelength was held fixed while a small ac voltage was placed across the sample in addition to the dc bias, which was varied. The fundamental and second-harmonic ac components of the PC were measured with a lock-in amplifier. These components are proportional, respectively, to the first and second derivatives of the PC with respect to the bias voltage.

3. Results

Figure 3(a) shows the PL spectrum at 2 K for each of the five samples studied. The interband threshold energy E_0 and the PL FWHM ΔE_{PL} are determined from these spectra and recorded in columns 4 and 5, respectively, of table 1, along with other pertinent information. In figure 3(b), the measured PL FWHM is plotted versus the theoretically predicted linewidth calculated according to the alloy broadening model described elsewhere [6]. We find satisfactory agreement between measurement and theory over a wide range of PL linewidths, indicating that alloy fluctuations are the dominant mechanism for PL linewidth broadening in these superlattices.

Figure 4(a) is an example PC spectrum for sample c. The spectrum was recorded at a constant energy excitation of 1.016 eV and a variable applied bias. Because the excitation energy is less than the zero-field interband transition energy of 1.088 eV, there is no PC observed at zero electric field. As shown schematically in figure 4(b), PC maxima occur at applied electric fields when the oblique interband transition energies of the superlattice become coincident with the excitation energy. An interband transition between wells separated by n superlattice periods is denoted by a Stark-ladder index n. The Stark-ladder indices n corresponding to PC maxima are labeled in figures 4(a) and (b). The inset of figure 4(a) (solid line) magnifies the

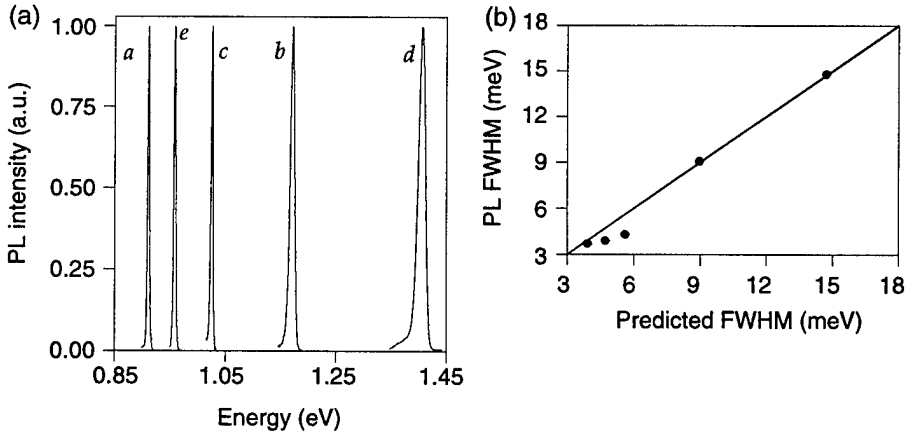

Figure 3. Photoluminescence data at 2 K for samples a through e: (a) PL spectra: interband threshold energy E_0 is taken as PL peak. (b) Measured PL FWHM from (a) versus theoretically predicted FWHM from alloy-broadening model of reference 6.

Table 1. Structural and optical characteristics of samples considered in this study.

Sample	Barrier-to-well ratio (Å)	Miniband width (meV)	Interband threshold energy E_0 (eV)	PL FWHM (meV)	Largest Stark-ladder index at energy E (eV)	Well-to-well drop (meV)	Ratio of col 7/col 5
a	53.6/16.4	61	0.943	3.7	$n = -7$ at 0.901	6.0	1.43
b	36.6/18.4	64	1.21	9.1	$n = -4$ at 1.170	12.5	1.10
c	20/30	120	1.088	4.3	$n = -14$ at 1.024	4.9	1.14
d	43.3/6.7	110	1.480	14.8	$n = -4$ at 1.397	20.8	1.40
e	17/40	80	1.010	3.9	$n = -11$ at 0.955	5.0	1.28

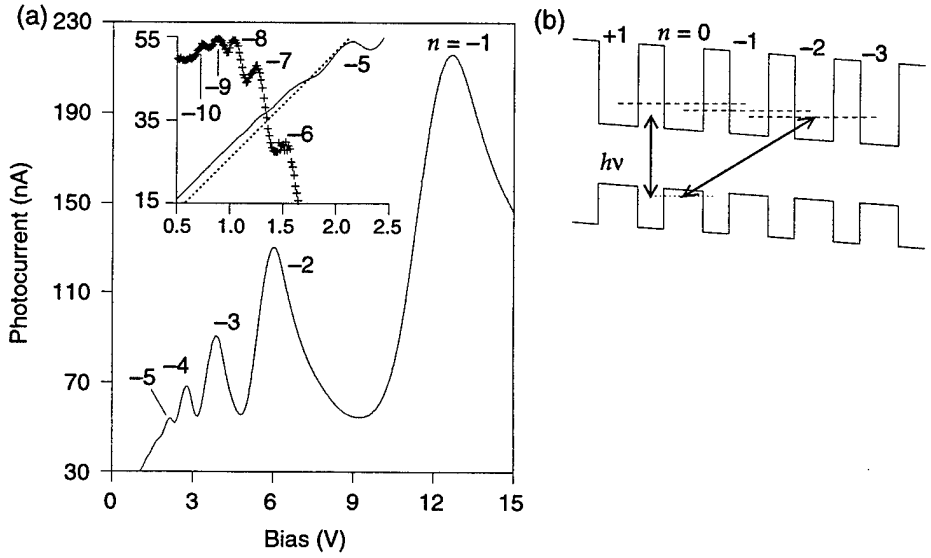

Figure 4. Photoabsorption processes for sample *c*: (a) Photocurrent spectrum of sample *c* taken with below-threshold optical excitation of 1.016 eV and variable applied bias. Wannier-Stark ladder transitions n are labeled. Inset: magnified view of low-bias region of spectrum (see text), showing oblique Wannier-Stark transitions up to $n = -10$. (b) Schematic diagram of oblique optical absorption processes.

low-bias region of the spectrum. The dotted line in the inset is an arbitrarily chosen straight line, and the plotted crosses are the rescaled difference between the spectrum and the dotted line. The crosses reveal oblique optical transitions between wells separated by up to 10 superlattice periods, or 500 Å.

It should be clear, however, that the sensitivity of the PC method to the oblique Wannier-Stark transitions is limited. The inset of figure 4(a) illustrates that one is eventually reduced to looking for small maxima on top of

large dc PC signals. This circumstance suggests that derivative techniques would enhance the sensitivity to oblique transitions with high Stark-ladder indices.

Figure 5 shows PC, first-derivative, and second-derivative spectra at an excitation energy of 1.024 eV for sample *c*. The spectra are plotted as a function of F^{-1}. The PC spectrum (fig. 5(a)) shows oblique transitions of Stark-ladder index up to $n = -8$. The first-derivative spectrum (fig. 5(b)) clearly shows features out to $n = -14$. These results are corroborated by the second-derivative spectrum (c), which also contains features out to $n = -14$. Note that the maxima of the PC spectra correspond to zeroes (with positive slope) in the first-derivative spectra, and to minima in the second-derivative spectra. Note also that the maxima and minima occur periodically as a function of F^{-1}, which corroborates the Wannier-Stark origin of these oscillations.

Because of the large heavy-hole mass, heavy-hole superlattice states are confined to a single well even near zero electric field. Thus, the observation of oblique optical transitions corresponds to a measurement of the spatial extent of conduction band Wannier-Stark states. The $n = -14$ Stark-ladder transition for sample *c* is observed at a field of 10 kV/cm. This field corresponds to a well-to-well potential drop of 4.9 meV. At such small electric fields, the electron wavefunction is approximately symmetric about the central quantum well. For example, the electron envelope wavefunction plotted in figure 1(b) is calculated with the well and barrier thicknesses of sample *c*, and an electric field of 28 kV/cm. Thus, the observation of the $n = -14$ Stark-ladder transition indicates that the electron wavefunction extends over 29 superlattice periods, or 1450 Å.

PC, first-derivative, and second-derivative spectra were also measured for the other four samples. For each of these samples, we determined the well-to-well potential drop corresponding to the highest Stark-ladder transition observed. These results are recorded in column 7 of table 1.

The last column of numbers in table 1 is the ratio of the well-to-well potential drop at the onset of Stark-localized behavior (column 7) to the measured PL linewidth (column 5). The numbers in this column vary between 1.10 (sample *b*) and 1.43 (sample *a*). For all samples studied, we find that the Wannier-Stark ladder becomes observable when the well-to-well potential drop is between 1.1 and 1.43 times the PL linewidth. This observation validates the intuitive picture proposed for the transition between the miniband and Wannier-Stark electric field regimes.

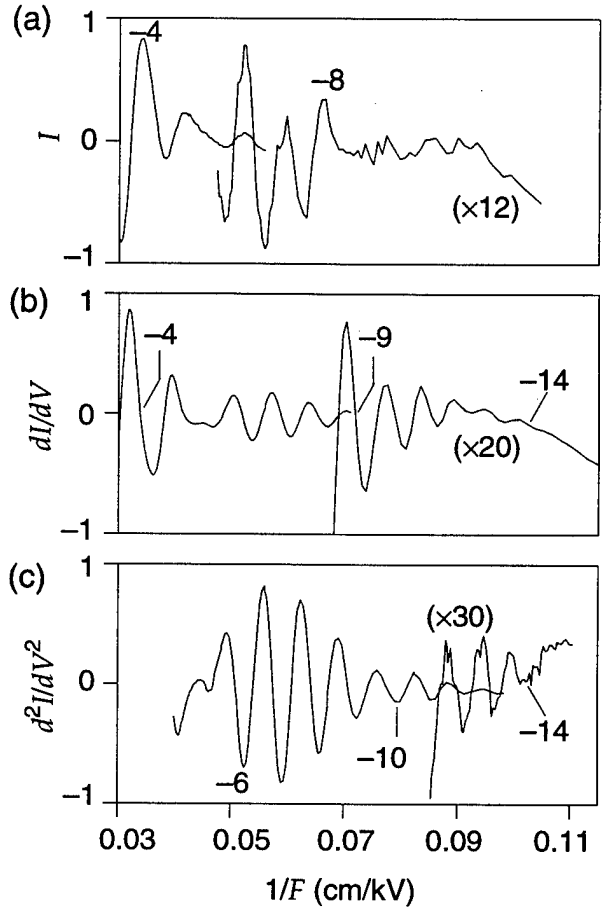

Figure 5. Spectra of superlattice sample e at an excitation energy of 1.024 eV: (a) photocurrent, (b) first derivative, and (c) second derivative. Wannier-Stark ladder transitions n are labeled.

4. Summary and Conclusions

We have shown that the spatial coherence length of electron wavefunctions can be accurately measured by means of first- and second-derivative PC spectroscopy. We note in particular the results for samples c and e. The largest Stark-ladder index observed for these superlattices is $n = -14$ and -11, respectively. This corresponds to spatial extents of the electron wavefunctions of 29 and 23 superlattice periods, or 1450 and 1310 Å, respectively. These coherence lengths are longer than the longest yet reported in the literature [7–9].

In all samples studied, we find that the superlattice miniband breaks up into the Wannier-Stark ladder when the well-to-well potential drop in the superlattice is between 1.1 and 1.43 times the low-temperature PL linewidth. Furthermore, the PL linewidths of all the samples studied are in reasonable agreement with a simple theoretical treatment [6] of linewidth broadening due to alloy fluctuations of the constituent superlattice materials.

These results confirm the following intuitive picture for the transition between the miniband and Wannier-Stark ladder electric field regimes in $In_{0.53}Ga_{0.47}As/In_{0.52}Al_{0.48}As$-on-InP superlattices. At zero electric field the superlattice electron states are localized. This localization is due to random fluctuations of the alloy potential and layer thickness fluctuations that underlie the observed PL linewidth. Thus, electric field effects associated with the Wannier-Stark regime are observed only when the Stark localization length Δ/eF is smaller than the coherence length of the electronic states localized by the random potential.

Acknowledgments

We gratefully acknowledge helpful discussions with J. D. Bruno, E. E. Mendez, and H. Kurz; we thank J. T. Pham and L. Lucas for sample processing.

References

1. W. A. Beck, J. A. Little, A. C. Goldberg, and T. S. Faska, *LWIR imaging using miniband transport multiple quantum well infrared detectors,* Proceedings of the First International Symposium on Long Wavelength Infrared Detectors, The Electrochemical Society, New Orleans, LA (October 1993).

2. K. K. Choi, M. Dutta, P. G. Newman, M.-L. Saunders, and G. J. Iafrate, *10 μm infrared hot-electron transistors,* Appl. Phys. Lett. **57**, 1348 (1990); K. K. Choi, M. Dutta, R. P. Moekirk, C. H. Kuan, and G. J. Iafrate, *Application of superlattice bandpass filters in 10 μm infrared detection,* Appl. Phys. Lett. **58**, 1533 (1991); K. K. Choi, L. Fotiadis, M. Taysing-Lara, and W. Chang, *High detectivity InGaAs base infrared hot-electron transistor,* Appl. Phys. Lett. **59**, 3303 (1991).

3. M. Stead, G. J. Simonis, J. Pham, R. Leavitt, F. Towner, and N. Gupta, *50-dB integratable self-aligned Stark-ladder electroabsorption waveguide modulator,* IEEE Photon. Technol. Lett. **5**, 689–692 (1993).

4. J. L. Bradshaw and R. P. Leavitt, *Observation of an electron-wavefunction coherence length approaching the theoretical limit in a nearly ideal semiconductor-alloy superlattice,* Phys. Rev. B**50**, 17,666 (1994).

5. D. F. Nelson, R. C. Miller, and D. A. Kleinman, *Band nonparabolicity effects in semiconductor quantum wells,* Phys. Rev. B**35**, 7770 (1990).

6. R. P. Leavitt and J. L. Bradshaw, *Molecular-beam-epitaxial growth and characterization of high-quality alloys and multiple quantum wells on InP substrates using a post-evaporation-heated arsenic source,* J. Appl. Phys. **76**, 3429 (1994).

7. F. Agulló-Rueda, E. E. Mendez, and J. M. Hong, *Quantum coherence in semiconductor superlattices,* Phys. Rev. B**40**, 1357 (1989).

8. E. E. Mendez, F. Agulló-Rueda, and J. M. Hong, *Stark localization in GaAs-GaAlAs superlattices under an electric field,* Appl. Phys. Lett. **56**, 2545 (1990).

9. K. H. Schmidt, N. Linder, G. H. Döhler, H. T. Grahn, K. Ploog, and H. Schneider, *Coexistence of Wannier-Stark transitions and miniband Franz-Keldysh oscillations in strongly coupled GaAs-AlAs superlattices,* Phys. Rev. Lett. **72**, 2769 (1994).

Distribution

Admnstr
Defns Techl Info Ctr
Attn DTIC-OCP
8725 John J Kingman Rd Ste 0944
FT Belvoir VA 22060-6218

Dept of Defns
Attn R222 J Fitz
4800 Savage Rd
FT Meade MD 20755-6000

Ofc of the Dir Rsrch and Engrg
Attn R Menz
Pentagon Rm 3E1089
Washington DC 20301-3080

Ofc of the Secy of Defns
Attn ODDRE (R&AT) G Singley
Attn ODDRE (R&AT) S Gontarek
The Pentagon
Washington DC 20301-3080

OSD
Attn OUSD(A&T)/ODDDR&E(R) J Lupo
Washington DC 20301-7100

CECOM
Attn PM GPS COL S Young
FT Monmouth NJ 07703

CECOM RDEC Elect System Div Dir
Attn J Niemela
FT Monmouth NJ 07703

CECOM
Sp & Terrestrial Commctn Div
Attn AMSEL-RD-ST-MC-M H Soicher
FT Monmouth NJ 07703-5203

Dir of Assessment and Eval
Attn SARD-ZD H K Fallin Jr
103 Army Pentagon Rm 2E673
Washington DC 20301-0163

MICOM RDEC
Attn AMSMI-RD W C McCorkle
Redstone Arsenal AL 35898-5240

US Army ARDEC
Attn AMSTA-FSF-RE B95 N H A Jenkinson
Picatinny Arsenal NJ 07806-5000

US Army Avn Rsrch, Dev, & Engrg Ctr
Attn T L House
4300 Goodfellow Blvd
St Louis MO 63120-1798

US Army CECOM
Attn AMSEL-RD-ST-LA-F L A Coryell
FT Monmouth NJ 07703-5000

US Army CECOM Rsrch, Dev, & Engrg
Attn R F Giordano
FT Monmouth NJ 07703-5201

US Army Edgewood Rsrch, Dev, & Engrg Ctr
Attn SCBRD-TD J Vervier
Aberdeen Proving Ground MD 21010-5423

US Army Info Sys Engrg Cmd
Attn ASQB-OTD F Jenia
FT Huachuca AZ 85613-5300

US Army Materiel Sys Analysis Agency
Attn AMXSY-D J McCarthy
Aberdeen Proving Ground MD 21005-5071

US Army Matl Cmnd
Dpty CG for RDE Hdqtrs
Attn AMCRD BG Beauchamp
5001 Eisenhower Ave
Alexandria VA 22333-0001

US Army Matl Cmnd
Prin Dpty for Acquisition Hdqrts
Attn AMCDCG-A D Adams
5001 Eisenhower Ave
Alexandria VA 22333-0001

US Army Matl Cmnd
Prin Dpty for Techlgy Hdqrts
Attn AMCDCG-T M Fisette
5001 Eisenhower Ave
Alexandria VA 22333-0001

US Army Mis Cmnd
Attn AMSMI-RD-WS P Ashley
Attn AMSMI-RD-WS-PO J L Johnson
Attn AMSMI-RD-WS-ST M J Bloemer
Huntsville AL 35898

Distribution

US Army Natick Rsrch, Dev, & Engrg Ctr
Acting Techl Dir
Attn SSCNC-T P Brandler
Natick MA 01760-5002

US Army Rsrch Ofc
Attn J Harvey
Attn M Dutta
Attn H Everitt
Attn M Stroscio
Attn J Zavada
PO Box 12211
Research Triangle Park NC 07709-2211

US Army Simulation, Train, & Instrmntn Cmd
Attn J Stahl
12350 Research Parkway
Orlando FL 32826-3726

US Army Tank-Automtv & Armaments Cmd
Attn AMSTA-AR-TD C Spinelli
Bldg 1
Picatinny Arsenal NJ 07806-5000

US Army Tank-Automtv Cmd
Rsrch, Dev, & Engrg Ctr
Attn AMSTA-TA J Chapin
Warren MI 48397-5000

US Army Test & Eval Cmd
Attn R G Pollard III
Aberdeen Proving Ground MD 21005-5055

US Army Train & Doctrine Cmd
Battle Lab Integration & Techl Dirctrt
Attn ATCD-B J A Klevecz
FT Monroe VA 23651-5850

USAASA
Attn MOAS-AI W Parron
9325 Gunston Rd Ste N319
FT Belvoir VA 22060-5582

Nav Surface Warfare Ctr
Attn Code B07 J Pennella
17320 Dahlgren Rd Bldg 1470 Rm 1101
Dahlgren VA 22448-5100

GPS Joint Prog Ofc Dir
Attn COL J Clay
2435 Vela Way Ste 1613
Los Angeles AFB CA 90245-5500

DARPA
Attn B Kaspar
Attn L Stotts
3701 N Fairfax Dr
Arlington VA 22203-1714

ARL Electromag Group
Attn Campus Mail Code F0250 A Tucker
University of Texas
Austin TX 78712

Univ of MD Elect Engrg
Attn A Christou
Attn C Davis
Attn M Dagenais
College Park MD 20742

Univ of MD Elect Engrg Dept
Attn R Chen
Baltimore County
Catonsville MD 21228

Dir for MANPRINT
Ofc of the Deputy Chief of Staff for Prsnnl
Attn J Hiller
The Pentagon Rm 2C733
Washington DC 20301-0300

Inst for Microstructural Sci Natl Rsrch Council
of Canada
Attn E Koteles
Attn H C Liu
Building 23 A Montreal Rd
Ottawa Ontario K1A OR6
Canada

NIST
Attn J Comas
Gaithersburg MD 20899

Distribution

US Army Rsrch Lab
Attn AMSRL-CI-LL Techl Lib (3 copies)
Attn AMSRL-CS-AL-TA Mail & Records Mgmt
Attn AMSRL-CS-AL-TP Techl Pub (3 copies)
Attn AMSRL-SE-E D Wilmot
Attn AMSRL-SE-E J Pellegrino
Attn AMSRL-SE-EE S Kennerly
Attn AMSRL-SE-EE Z G Sztankay
Attn AMSRL-SE-EI B Beck
Attn AMSRL-SE-EI W Clark
Attn AMSRL-SE-EI N Dhar
Attn AMSRL-SE-EI E Poindexter
Attn AMSRL-SE-EM A Goldberg
Attn AMSRL-SE-EM B Riely
Attn AMSRL-SE-EM D Smith
Attn AMSRL-SE-EM D Wortman
Attn AMSRL-SE-EM F Semendy
Attn AMSRL-SE-EM G Simonis
Attn AMSRL-SE-EM J Bradshaw (25 copies)

US Army Rsrch Lab (cont'd)
Attn AMSRL-SE-EM J Bruno
Attn AMSRL-SE-EM J Little
Attn AMSRL-SE-EM J Pamulapati
Attn AMSRL-SE-EM J Pham
Attn AMSRL-SE-EM K K Choi
Attn AMSRL-SE-EM K Oliver
Attn AMSRL-SE-EM K Ritter
Attn AMSRL-SE-EM L Lucas
Attn AMSRL-SE-EM M Stead
Attn AMSRL-SE-EM M Tobin
Attn AMSRL-SE-EM P Folkes
Attn AMSRL-SE-EM P Taylor
Attn AMSRL-SE-EM R Leavitt (10 copies)
Attn AMSRL-SE-EM R Tober
Attn AMSRL-SE-EM S Rudin
Attn AMSRL-SE-EM T B Bahder
Attn AMSRL-SE-EO J Mait
Attn AMSRL-SE-EO J Van der Gracht
Attn AMSRL-SE H Pollehn
Adelphi MD 20783-1197

REPORT DOCUMENTATION PAGE

Form Approved
OMB No. 0704-0188

1. AGENCY USE ONLY *(Leave blank)*	2. REPORT DATE	3. REPORT TYPE AND DATES COVERED
	February 1998	progress, from June 1994 to Sep 1997

4. TITLE AND SUBTITLE
The Spatial Coherence of Electron Wavefunctions and the Transition from Miniband to Stark-Ladder Electric Field Regimes in InGaAs/InAlAs-on-InP Superlattices

5. FUNDING NUMBERS
PE: 61102A

6. AUTHOR(S)
John L. Bradshaw and Richard P. Leavitt

7. PERFORMING ORGANIZATION NAME(S) AND ADDRESS(ES)
U.S. Army Research Laboratory
Attn: AMSRL-SE-EM (johnlb@arl.mil)
2800 Powder Mill Road
Adelphi, MD 20783-1197

8. PERFORMING ORGANIZATION REPORT NUMBER
ARL-TR-1536

9. SPONSORING/MONITORING AGENCY NAME(S) AND ADDRESS(ES)
U.S. Army Research Laboratory
2800 Powder Mill Road
Adelphi, MD 20783-1197

10. SPONSORING/MONITORING AGENCY REPORT NUMBER

11. SUPPLEMENTARY NOTES
AMS code: 611102.H44
ARL PR: 7NE3GG

12a. DISTRIBUTION/AVAILABILITY STATEMENT
Approved for public release; distribution unlimited.

12b. DISTRIBUTION CODE

13. ABSTRACT *(Maximum 200 words)*

Five $In_{0.53}Ga_{0.47}As/In_{0.52}Al_{0.48}As$-on-InP superlattices of various well-to-barrier ratios and miniband widths have been studied by low-temperature photoluminescence, photocurrent, and differential photocurrent spectroscopies. These techniques provide a means of measuring the spatial coherence length of electron wavefunctions in the superlattices. We find that the onset of Wannier-Stark localization occurs when the well-to-well potential drop within the superlattice is between 1.1 and 1.43 times the low-temperature photoluminescence linewidth for all samples studied. Furthermore, the photoluminescence linewidth is accurately describable in terms of a simple model for alloy broadening. These findings confirm an intuitive picture for the transition between the miniband and Wannier-Stark electric field regimes in $In_{0.53}Ga_{0.48}As/In_{0.52}Al_{0.48}As$-on-InP superlattices.

14. SUBJECT TERMS	15. NUMBER OF PAGES
Coherence, superlattice	25
	16. PRICE CODE

17. SECURITY CLASSIFICATION OF REPORT	18. SECURITY CLASSIFICATION OF THIS PAGE	19. SECURITY CLASSIFICATION OF ABSTRACT	20. LIMITATION OF ABSTRACT
Unclassified	Unclassified	Unclassified	UL

NSN 7540-01-280-5500

Standard Form 298 (Rev. 2-89)
Prescribed by ANSI Std. Z39-18
298-102